Military Technical College
Kobry El-Kobbah,
Cairo, Egypt.

18th International Conference on Applied Mechanics and Mechanical Engineering.

EXPERIMENTAL AND FINITE ELEMENT ANALYSIS OF BOLT-HOLE CLEARANCE EFFECTS IN COMPOSITE JOINTS

U. A. Khashaba[a,b,*], T. A. Sebaey[b] and Al Selmy[b]

ABSTRACT

Bolt-hole clearance effects on bearing strength of bolted joints in cross-ply, $[0/90]_{2s}$, glass fiber reinforced epoxy (GFRE) composites, were investigated experimentally and numerically. A series of ASTM tests (tensile, compressive and shear) were conducted on a unidirectional laminates to find the lamina properties, which were used as input to a 3D developed progressive damage model (PDM). The model was built with the aid of ABAQUS software, nonlinear Hashin failure criteria and Riccio property degradation rules. The PDM was used to predict the failure load and mode of composite bolted joint with bolt-hole clearance of 0, 50, 100, 200, 300 µm. Bearing strength was determined according to three different criteria: load at 4% hole deformation, first peak load and ultimate load. The numerical results of the ultimate strength agree well with the experimental ones with a maximum deviation of 7.1 %. Increasing the bolt-hole clearance from 0 to 300 µm reduces the contact area by 17.8% and increasing the contact pressure by 26.6 %. Accordingly, the 4% HDS, first peak bearing strength, the measured ultimate strength and the predicted ultimate strength were decreased respectively by 20.9%, 34.0%, 14.2% and 8.8%. On the other hand, the failure mode did not affected by increasing the bolt-hole clearance within the investigated values.

KEYWORDS

Bolted joint, Cross-ply GFRE composite, ABAQUS, Clearance, Nonlinear Hashin failure criteria, Property degradation rules.

[a] Mechanical Engineering Department, Faculty of Engineering, King Abdulaziz University, P.O. Box 80204, Jeddah 21589, Saudi Arabia
[b] Mechanical Design and Production Engineering Department, Faculty of Engineering, Zagazig University, P.O. Box 44519, Zagazig, Egypt
[*] Corresponding author. Tel.: +966553507515; Fax: +96626952181. *E–mail addresses*: khashabu@zu.edu.eg, khashabu@hotmail.com (U.A. Khashaba).

INTRODUCTION

The combination of high specific strength and specific stiffness as well as impact resistance gives to the glass fiber reinforced polymer (GFRP) composites a great advantage for automotive and space applications. Among the different techniques of joining composite members, mechanical fastening through a pin is a common choice because of low cost, simplicity and facilitation of disassembly for repair. On the other hand, the stress concentrations near the fastener holes can be the initiators for a variety of failure modes such as: (1) local bearing, (2) net tension, (3) wedge-type splitting, (4) shear-out, and (5) tension with shear-out [1,2]. The approximate equations used to quantify these failure modes are described in detail by Chamis [2].

Bearing strength is defined as the value of bearing stress occurring at a significant event on the bearing stress-bearing strain curve [3]. The various bearing failure criteria, include: (a) 2% offset bearing strength criterion [4], ASTM D D5961, (b) first peak load of load-pin displacement curve [5-7], (c) bearing failure as the maximum load just prior to unstable, nonlinear behavior [8], (d) 4% hole deformation strength (HDS) [9], ASTM D953, (e) ultimate failure loads [1,9,10], (f) ultimate bearing strain [11], and (g) a 5% stiffness drop has been proposed by Camanho and Lambert [12]. The actual definition of the bearing strength is not going to influence the output of this study in which the bearing stresses were determined at the first peak load, ultimate load and 4% hole deformation load.

A better understanding of the bolted joint behavior is essential to the design of efficient automotive and aerospace structures from FRP composite materials. In practical applications, the diameter of fasteners and holes are within certain allowed tolerances. The combination of bolt and hole tolerances result in a range of allowable bolt-hole fits, which in composites are generally clearance rather than interference fits, due to concerns over damage caused to the composite during insertion of the fastener, and also possibly removal of the fastener during inspections [11]. The demands for improving the performance of the bolted joints in composite structures are required forever and remain open for further research.

Experimental testing and numerical modeling have been provided valuable insight to the behavior of bolted joint in composite structures by many investigators [9, 13-16] and is the subject of the present work. Hyer et al. [13] investigated the effects of pin elasticity, clearance and friction on the stress state of pin-loaded joints. The effects of friction and clearance were found to be most significant affecting both the distribution and magnitude of the stresses around the hole. Clearances of 0 (neat fit) and 40 μm were considered for a nominal hole diameter of 4 mm. The 40 μm clearance resulted in a reduction of the contact angle by 22% with a corresponding reduction in the predicted joint strength of 12%.

Kelly and Hallström [9] reported that the magnitude and distribution of stress at the hole was found to be significantly dependent on the level of bolt-hole clearance in carbon fiber/epoxy composite joints. Increasing the bolt-hole clearance was found to be significant reduction the 4% HDS. However, the ultimate strength of the laminates illustrated no dependency on the bolt-hole clearance. Hu et al. [15] reported that during bearing failure, the external load may reach a plateau while the local bearing strain around the bolt-hole continues to increase considerably (zero stiffness response) due to significant material failure by crushing. Finite element modeling

often fails to capture the zero stiffness response due to the complex contact geometries/interaction of the bolt surfaces with surrounding structure and nonlinearities owing to material damage and failure. McCarthy et al. [14] investigated the effect of clearance between the bolt and the hole using angle-ply high tensile strength carbon fiber reinforced epoxy laminates. A three dimension frictional contact model investigated to simulate the problem with an interface with the ABAQUS software. From the finite element model, it was found that increasing clearance had the effect of reducing the stiffness of single-bolt joint.

The present work is a continuation of an earlier paper by the authors [17] wherein the failure load and mode in composite bolted joints with different stacking sequences and zero bolt-hole clearance (neat-fit) was studied experimentally and numerically.In the current study, a series of ASTM tests (tension, compression and shear) were performed on a unidirectional laminates to determine the lamina mechanical properties. The failure loads and modes of bolted joints in cross-ply laminates were determined at different bolt-hole clearances of 0, 50, 100, 200, 300 µm in accordance with ASTM D5961. The failure modes of both the mechanical characterization tests and the bolted joint tests were compared with the ASTM standards. A progressive damage model was developed using the ABAQUS software, nonlinear Hashin failure criteria and Riccio property degradation rules to predict the failure load and mode of bolted joints in the GFRE laminates.

EXPERIMENTAL WORK

Specimen Manufacturing and Preparation

Unidirectional (UD) $[0]_8$ and cross-ply $[0/90]_{2S}$ composite laminates with 3.2±0.1 mm thickness were fabricated from eight layers of E-glass fiber reinforced epoxy using the hand lay-up technique. The constituent materials of composite laminates are illustrated in Table 1. Details about the manufacturing technique were presented elsewhere, Khashaba et al. [18]. The fiber volume fraction of the fabricated laminates (40 ± 0.5 %) was determined experimentally using the ignition technique according to ASTM D3171.

Table 1. The constituent materials of GFRE laminate.

Materials	Properties
Fiber	E-roving glass fiber linear density = 2.10 g/m, d = 17 ± 2 µm Density = 2.54 g/cm^3
Matrix	Epoxy resin: Araldite PY 1092 (100 part by weight); Hardener HY 1092 (50 part by weight) Density 1.1 g/cm^3

Tensile, Compression and In-Plane Shear Tests

A series of ASTM tests are performed on the UD-GFRE laminates to determine the tensile and compressive properties in the longitudinal and transverse directions. In

addition, Iosipescu shear tests were conducted to determine the in-plane shear properties (strength and modulus) normal to the fiber direction. At least five specimens were tested for each experiment as shown in Table 2. All tests were performed using computer controlled Testometric 200 KN universal testing machine. The cross-head speed of tension, compression and in-plane shear tests were respectively 2, 1.3 and 2 mm/min. The specimen dimensions for each test type were determined in accordance with the ASTM standards as shown in Table 2.

Table 2. Geometry and required number of test specimens.

Test	No. of Specimens	Specimen dimensions	Determinable Parameters	Test Method
Tensile	5	I- In the Fiber direction 250x25x3.2 mm (Gauge length = 138-mm) Four rectangle aluminum end tabs were bonded to the gripping length (56-mm)	E_1 v_{12} X_t	ASTM D 3039
	5	II- Perpendicular to the Fiber direction 250x25x3.2 mm (Gauge length = 138-mm) Four rectangle aluminum end tabs were bonded to the gripping length (56-mm)	E_2 Y_t	ASTM D 3039
Compression	5	I- In the Fiber direction 80x17x3.2 mm (Gauge length = 5-mm) Four rectangle aluminum end tabs were bonded to the gripping length (37.5-mm)	X_C	ASTM D695
	5	II- Perpendicular to the Fiber direction 80x17x3.2 mm (Gauge length = 5-mm) Four rectangle aluminum end tabs were bonded to the gripping length (37.5-mm)	Y_C	ASTM D695
Shear	7	Double V-notch specimen 75x19x3.2 (Gauge length = 11.4-mm)	G_{12} α S	ASTM D 5379

The true Young's moduli (E_1 and E_2) and Poisson's ratio in the tensile tests were measured using two like strain gauges bonded back to back on the specimen center. The strain gauges are connected with two-channel digital strain meter model (model Tc-21K 232). Iosipescu shear tests fixture and double V-notch specimens were used to measure the shear strain (γ_{xy}) and shear modulus (G_{xy}) of the UD-GFRE laminate. Two strain gauges were bonded at ±45 o ahead of the V-notches at the center of the test specimen as shown in Fig. 1. Details on the test procedure are illustrated earlier, Khashaba et al. [19].

Bolted Joint Tests

The strength of bolted joints was determined experimentally according to ASTM D5961. The bolt diameter (D) was equal to 6 mm. The e/d = 3 and w/d = 6 ratios were kept constant in all specimens as shown in Fig. 2a. The bolted joint test fixure were manufactured from stainless steel according to the geometry illustrated in Fig. 2b, ASTM D5961. The selected clearance values are: 0, 50, 100, 200 and 300 μm, which are coded respectively from C1 to C5. The varying bolt-hole clearances were obtained by using constant diameter bolts of 6-mm and various hole diameters [20].

Clearance values of C1 and C2 are within current aerospace tolerances (≤ 75 μm, f7/H10 ISO fitting [21]), C3 is slightly outside and the latter two clearance values (C4 and C5) are used to study the possible effects of out-of tolerance on the failure load and mode in the composites bolted joints [22].

The value of ultimate strength, in bearing test, was calculated by dividing the fracture load by the projected area of the hole. Because of the first peak bearing load is clearly observed on the load-displacement curves of the joints, it was selected as a bolt failure criterion for calculating the bearing strength of the bolted joints. The actual thickness (in the vicinity of the hole) and hole diameters for each individual joint were used in the calculations of bearing strength, ASTM D 5961. At least, five tests were implemented for each clearance value. The mechanical tests as well as bolted joint tests were performed on computer controlled universal testing machine (model Testometric 200 kN) at crosshead speed of 2 mm/min.

PROGRESSIVE DAMAGE FE MODEL

In the present work a 3-D progressive damage model (PDM) was developed to predict the failure mode and load in composite bolted joint with different bolt/washer diameter and subjected to varying tightening torque values. The developed PDM will be used, in this study, to predict the 0.4% hole deformation strength (HDS) and the ultimate strength of pin-hole joint (zero torque) with different clearance values in cross-ply laminate. Failure mode in the composite layers of the bolted composite joint was predicted using the developed PDM. The effect of washer size and tightening torque will be investigated in the following paper.

Problem Formulation

A 3-D progressive damage model was built with the aid of ABAQUS software, nonlinear Hashin failure criteria and Riccio property degradation rules to predict the failure load and mode of bolted joints in GFRE laminates. The developed model is simple and computationally non-expensive, which is adopted by assuming that: no delamination effect, constant bolt-hole coefficient of friction of 0.1, quasi-static (load is time dependent), and non-viscoelastic conditions (material characteristics are time independent). More details about the developed FE model can be found in previous studies [17] and is only outlined briefly here.
The boundary Ω is assumed to consist of three disjoint measurable parts Γ_C, Γ_D and Γ_F on which displacement and traction are prescribed, Fig. 3. The parts are meshed using the 8-node linear isoperimetric element. Γ_C is the candidate contact zone containing the adjacent contact interfaces. Fixed constraints are made on the bolt heads Γ_{D1}. A very important fixed constraint is applied to the surface of the plate Γ_{D2} to simulate the contact between the specimen and the machine jaws. The latter fixed constraint allows the nodes to deform in the loading direction only. A uniform distributed load is applied on the specimen via machine grip, Γ_F. A frictional contact boundary condition is applied between the bolt and the hole and between the bolt heads and the outer layers, Γ_C, Fig. 3. The Augmented Lagrange method is used to simulate contact behavior. The contacting nodes are allowed to separate after contact. The detailed contact algorithm can be seen elsewhere [23]. The ABAQUS perform the stress analysis then, with a certain interaction between the ABAQUS and the subroutine USDFLD, the model performs a failure analysis using the nonlinear

Hashin failure criteria. If a failure detected at any integration point, the properties of this element was degraded by means of the Riccio property degradation rules. The model is explained by means of the flowchart in Fig. 4.

Boundary Conditions

The traction boundary conditions contain the pressure applied to the free end of the specimen and the clamping pressure under the washer. In order to simulate the bolt preload (tighten torque), a shrink fit is to be considered between the bolt head and the outer layers. This does not mean interpenetration, in the first contact step, before applying the load; this initial interpenetration will removed to produce a contact pressure between the two bodies [24]. In general form the traction boundary conditions can be expressed as:

$$P = \sigma_{ij}\, n_i\, n_j \qquad (on \quad \Gamma_F) \tag{1}$$

The prescribed displacement boundary conditions can be expressed as:

$$U_i = 0 \begin{cases} i = 1,\ 2, 3 & (on \quad \Gamma_{D1}) \\ i = 2, 3 & (on\ \ \Gamma_{D2}) \end{cases} \tag{2}$$

The first equation represents the fixation of the bolt head and the second one represents the clamping of the specimen free end in the movable machine grip. In order to simulate the bolt preload (tighten torque), a shrink fit is to be considered between the bolt head and the outer layers.

Candidate Contact Boundary Conditions

Throughout the contact interfaces, the relative displacement in the normal and tangential directions between the candidate contact pair nodes *II* and *I* are given by:

$$\begin{aligned} \Delta U_n &= (U_i n_i)^{II} - (U_i n_i)^{I} \qquad (On \quad \Gamma_C) \\ \Delta U_t &= (U_t)^{II} - (U_t)^{I} \qquad (\mathrm{On} \quad \Gamma_C) \end{aligned} \tag{3}$$

where *I* and *II* refer to the two contacting bodies, ΔU_n is the relative normal displacement between the contact pair nodes and ΔU_t is the relative tangential displacement between the contact pair nodes.
The contact constraint condition take the following form:

$$\Delta U_n - g \le 0 \qquad (On\ \ \Gamma_C) \tag{4}$$

where *g* refer to the gap between the two contacting bodies

The normal stress (σ_n) is given by:

$$\left.\begin{aligned} \sigma_n &= \sigma_{ij} n_i n_j \ \le 0 \\ \sigma_n &\left(\Delta U_n - g\right) = 0 \end{aligned}\right\} \qquad (On \quad \Gamma_C) \tag{5}$$

The first equation indicates that the contact stress is always compressive, and the second equation represents a switch to identify either the contact pairs is in contact

or not. When a pair of nodes comes into contact, the relative displacement ($\Delta U_n - g$) is zero, and hence the contact stress σ_n is nonzero and vice versa.

According to the classical Coulomb's law, the frictional stress can be evaluated as follows:

$$\tilde{\sigma}_t = \mu|\sigma_n|\,\tilde{t} \qquad on\ \ \Gamma_C \tag{6}$$

where $\tilde{\sigma}_t$ is the tangential stress vector, $\tilde{t}$ is the unit tangent to the adjacent contact interface, and μ is the static coefficient of friction.

3.4. Failure Criteria

The nonlinear Hashin failure criteria [25] with respect to failure modes are as follows:
Fiber tensile failure ($\sigma_{11} > 0$):

$$\left[\frac{\sigma_{11}}{X_t}\right]^2 + T \geq 1 \tag{7}$$

Fiber compressive failure ($\sigma_{11} < 0$):

$$\frac{|\sigma_{11}|}{X_c} \geq 1 \tag{8}$$

Matrix tensile failure ($\sigma_{22} > 0$):

$$\left[\frac{\sigma_{22}}{Y_t}\right]^2 + T \geq 1 \tag{9}$$

Matrix compressive Failure ($\sigma_{22} < 0$):

$$\left[\frac{\sigma_{22}}{Y_c}\right]^2 + T \geq 1 \tag{10}$$

where

$$T = \left(\frac{\tau_{12}}{S}\right)^2 \frac{1 + \frac{3}{2}\alpha G_{12}\tau_{12}^2}{1 + \frac{3}{2}\alpha G_{12}S^2} \tag{11}$$

and σ_{ij} are the stress components, X_t is the tensile strength in the fiber direction, Y_t is the tensile strength in the transverse direction, X_c is the compression strength in the fiber direction, Y_c is the compression strength in the transverse direction, S is the shear strength, τ_{12} is the in-plane shear stress, α is a nonlinear coefficient measured experimentally and G_{12} is the shear modulus of elasticity.

The degradation rules set most of the material properties of the failed portions to 0.1 of the non-failed properties (instead of zero) to avoid the convergence problems before the final failure of the problem, Table 3.

Through the present study the divergence of the solution was assumed to occur when the joint completely fail. Theoretically, the finite element method is a numerical technique so; we obtain a sequence of approximate solutions as the element size is

Table 3. Riccio material properties degradation rules.

Failure mode	Property degradation rules
Matrix tensile failure ($\sigma_2 \geq 0$)	$E_2^d = 0.1E_2$, $E_3^d = 0.1E_3$, $G_{23}^d = 0.1G_{23}$
Matrix compression failure ($\sigma_2 \leq 0$)	$E_2^d = 0.1E_2$, $E_3^d = 0.1E_3$, $G_{23}^d = 0.1G_{23}$
fiber tensile and compression failure	$E_1^d = 0.1E_1$

reduced successively. This sequence will converge to the exact solution if the inter polynomial satisfies two convergence requirements. The first one stated that the field variables must be continuous within the elements. The second stated that the element size must not reduce to zero [26]. From these two requirements we can return the failure of the joint to their large deformation zones.

EXPERIMENTAL RESULTS AND DISCUSSION

Tensile, compressive and in-plane shear properties (strength and modulus) of the UD-GFRE laminates were predicted from the mechanical properties of the constituent materials, Table 4, using well-known analytical models, Eqs. (12) to (22), as show in Table 5. This table also includes comparison between the predicted and the measured ones. The experimental results and failure modes are illustrated in the following subsections and discussed in the light of ASTM standards.

Table 4. Mechanical properties of E-glass fiber and Epoxy matrix.

property	E-glass fiber	Epoxy matrix
Volume fraction, V	0.4	0.6
Longitudinal modulus, E, GPa	74	3.35
In-plane shear modulus, G, GPa	30.8	1.24
Poisson's Ratio, v	0.2	0.35
Tensile Strength S_T, MPa	2150	73
Compressive strength, S_C, MPa	1450	97
Shear strength, S_S, MPa	--	67
Failure strain, ε, %	--	1.7

Tensile Results

Fig. 5a and b shows the tensile load-displacement diagrams of the UD-GFRE specimens in the longitudinal and transverse directions respectively. The ultimate tensile strengths were calculated from these curves. The average tensile strengths in the fiber direction, X_T, and perpendicular to the fiber direction, Y_T, are illustrated in Table 5. The longitudinal and transverse stress-strain curves of GFRE specimen loaded in the fiber direction are illustrated in Fig. 6a and b respectively. The strain values in this figure were obtained from the strain gauges. The actual Young's modulus in the fiber direction was determined at 0.5 % strain level [19] and presented in Table 5. The Poisson's ratio, v_{12}, is the ratio of the strain in the transverse direction to the strain in the longitudinal direction when the applied stress is in the longitudinal one. The measured Poisson's ratio from the stress-strain curve of Fig. 6a is (0.33) presented in Table 5. The measured strain in the transverse tensile test, Fig. 6b, is

Table. 5. Measured vs. calculated mechanical properties of UD-GFRE composite.

Property	Analytical model	Ref.	Eq. No.	Predicted value	Measured value	Standard deviation
E_1 (GPa)	$E_1 = E_m V_m + E_f V_f$	[27]	(12)	31.61	32.1	0.23
E_2 (GPa)	$E_2 = E_3 = \frac{E_f Em}{E_m V_f + E_f V_m}$	[27]	(13)	5.42	5.74	0.12
G_{12} (GPa)	$G_{12} = G_{13} = \frac{G_f G_m}{G_m V_f + G_f V_m}$	[27]	(14)	2.01	1.24	0.05
v_{12}	$\nu_{12} = \nu_{13} = \nu_m V_m + \nu_f V_f$	[27]	(15)	0.3	0.33	0.01
X_T (MPa)	$X_T \cong V_f \, S_{Tf}$	[27]	(16)	860	722	34.3
Y_T (MPa)	$Y_T = \frac{\varepsilon \, E_2}{F}$; *F* is the strain concentration factor = 3	[28]	(17)	32.5	14	3.35
X_C (MPa)	Fiber micro buckling in extension mode $X_C = 2 V_f \sqrt{\frac{V_f \, E_m \, E_f}{3 (1 - V_f)}}$	[29]	(18)	5937.8	238.19	38.1
	Fiber micro buckling in shear mode $X_C = \frac{G_m}{1 - V_f}$		(19)	2066.7		
	Fiber Kinking mode $X_C = \frac{G_m / (1 - V_f)}{1 + (\varphi / \gamma)}$; (φ / γ) = 4		(20)	413.34		
Y_C (MPa)	$Y_C = S_{Cm}\left[1 - (\sqrt{V_f} - v_f)\left(1 - \frac{E_m}{E_f}\right)\right]$	[27]	(21)	75.4	65	4.3
S (MPa)	$S = S_m\left[1 - (\sqrt{V_f} - V_f)\left(1 - \frac{G_m}{G_f}\right)\right]$	[27]	(22)	52.05	46	3.17

lower than the preferred value (0.5 %) for measuring the modulus and thus, it has determined from the slope of the initial linear portion up to 0.1% strain level as recommended by ASTM D 3039 (modulus can evaluated and reported at the user's discretion).

Fig. 7a shows the failure mode of UD-GFRE specimen loaded in the fiber direction. This failure mode can be described using three-part failure mode code as DGM, ASTM D3039. The first, second and third letters mean edge delamination, within the gauge length, and near the specimen middle, respectively, as shown in Fig. 7b. The

failure mode of UD-GFRE specimen loaded in the transverse to fiber direction is illustrated in Fig. 8a. This failure mode can be described using the three-part failure mode code as LGM, ASTM D3039, which mean lateral, within the gauge length, and near the specimen middle as shown in Fig. 8b. The visual examination of the fractured specimen showed smooth surface of debonded fibers accompanied with many fiber prints in the polymer matrix, which indicates a preferential mode of failure by interfacial debonding [30].

Compressive Results

Fig. 9a and b shows respectively, load-displacement curve and the failure mode of the UD-GFRE specimen in the longitudinal compression test. The ultimate compressive strength was calculated from this curve and the average value of the five tests is presented in Table 5. The failure mode is fiber kinging inside the gauge length of the specimen, which is agree well with the ASTM D 3410 (kinging-gauge-middle, KGM) typical failure mode, as shown in Fig. 9b.

Fig. 10a shows the load displacement curve of UD-GFRE specimen loaded in the transverse direction. The ultimate compressive strength in the transverse direction was calculated from this curve and the average of five values is presented in Table 5. The failure mode can be described, using the three characters theory, as HAT, ASTM D 3410. The initiation of failure occurs along the fiber/matrix interface which is controlled by shear stress generated between the fiber and matrix. The failure was at angle of about 44 ^{o}, Fig. 10b, which agrees well with the typical reported values, 45-56 ^{o}, by Gonzalez and Llorca [31].

Shear Results

Fig. 11a and b shows respectively, the load-displacement curve and failure mode of the UD-GFRE specimen in shear test. In defining shear strength, it is still debatable as to which load value should be used. Bhatanagar et al. [32] considered the first load drop to be the shear load responsible for material failure. Khashaba [19] defined shear strength as the ratio of the load just prior to the nonlinear behavior, to the cross-sectional area between the two notches of Iosipescu specimens. Some researchers defined the in-plane shear strength of Iosipescu specimens as the stress value corresponding to the ultimate load, which is more suitable for bolted joint failure criteria [33]. Thus, the ultimate shear strength was measured for seven specimens and the average value was illustrated in Table 5. The load-displacement curve of Fig. 11a showed a linear relationship, up to 60% of the ultimate load, and then followed by a nonlinear behavior due to matrix cracks, delamination at loading points and horizontal cracks parallel to the fiber directions ahead of the notch root, Fig. 11b. The deviation from the linearity was increased with increasing the applied load due to the propagation of shear cracks in the loading direction between the two V-notches. This failure mode is agreed well with the ASTM typical failure mode as shown in Fig. 11b.

Fig. 12a shows the shear stress vs strains of ±45° stain gauges. The shear strain (γ_{xy}) was calculated from Fig. 12a as [19]:

$$\gamma_{xy} = \varepsilon_{-45} - \varepsilon_{+45} \tag{23}$$

where ε_{+45} and ε_{-45} are the measured strains of +45° and -45° strain-gauges respectively.

The measured shear strains (γ_{12}) were used to draw the shear stress vs shear strain relationship as shown in Fig. 12b. From this figure, the true in-plane shear modulus was calculated from the slope of the initial linear portion of the shear stress-shear strain curve and the average value of seven test results is presented in Table 5.

The results in Table 5 showed that most of the measured mechanical properties are agree well with the predicted ones. The lower values of the measured tensile, compressive and shear strength was attributed to the higher exothermal heat (150°C) that was generated during the curing of the epoxy resin system [31]. Therefore, cure residual stress is contributed by the chemical shrinkage of the curing resin and the thermal cooling contraction of the resin and fiber system. Microscopically, the residual stresses are responsible for microcracking and fiber breakage. In addition, the voids contend in the composite laminate that formed during the manufacturing process can represent as stress initiator for fiber/matrix interfacial debonding as well as crack propagation and thus, reducing the laminate strength. On the other hand, the curing residual stress has no effect on the composite modulus, as reported by earlier, Zhao et al. [34].

Bolted Joint Results

Fig. 13 shows the load-displacement curve of bolted joint in $[0/90]_{2S}$ GFRE specimen with neat-fit clearance. The diagram was accompanied with some images that illustrate the failure sequence of the joint. It is evident that the joints have structural nonlinearity within small initial displacements until the bolt achieving full intimate contact with the hole at about 0.5 kN, and then followed by a linear relationship up to 3.6 kN. Matrix damage accompanied with delamination initiation was clearly observed at load of 2.3 kN. These damage mechanisms are progressively increased up to bearing and fiber splaying accompanied with shear-out initiations and a nonlinear behavior of the load-displacement curve at 3.6 kN as shown in Fig. 13. Bearing failure associated with shear-out was clearly observed at the first peak load of 5.35 kN. The fracture of the bolted joint was associated with net-tension failure mode at ultimate load of about 6.6 kN as shown in Fig. 13. The bolted joints with different clearance values are failed in the same manner of the neat-fit clearance one.

Fig. 14 shows the load-displacement curves of bolted joint in $[0/90]_{2S}$ GFRE specimens with different bolt-hole clearance values. Five test specimens were tested for each clearance value and the average values were compared with those predicted using the FE model as shown in the next section. It is evident from the load displacement curves of Fig. 14 that increasing the clearance up to C3 (100 μm) has insignificant effects on the stiffness of load-displacement curve. On the other hand, the stiffness as well as the first beak load and ultimate load were clearly decreased with increasing the bolt-hole clearance from 100 to 300 μm. Increasing the bolt-hole clearance from zero to 50 μm decreases the first peak and the ultimate strengths by 15.9 % and 6.2 %, respectively. Whereas, increasing the bolt-hole clearance from zero to 300 μm decreases the first peak and the ultimate strength by 34.0 % and 14.2 %, respectively. The main reason for decreasing the joint strength with increasing bolt-hole clearance is the decreasing of the contact angle/area and thus, increasing

the deformation and decreasing the stiffness of the bolted joint. Increasing the displacement of the bolted joints with larger clearances values was clearly observed in the load-displacement curves at any load levels. This behavior is more pronounced for constant loads larger than 4.0 kN as shown in Fig. 14.

NUMERICAL RESULTS AND DISCUSSION

Fig. 15 shows the measured and the numerical predicted bearing strength using different failure criteria. The results in this figure showed that the measured and predicted bolted joint strength are decreased with increasing bolt-hole clearance. The predicted ultimate strength of the bolted joint with different clearance values agrees very closely with those measured experimentally (maximum deviation = 7.1 %), Fig. 15. The predicted 4% hole deformation strength (HDS) was higher than the first peak strength by 6.4% for bolted joint with neat-fit. As the bolt-hole clearance varied from C2 to C5, the percent increase in the 4% HDS compared to the fist peak strength is in the range of 22 to 28.5%, as shown in Fig. 15. Almost the bolted joints with different clearance values are failed in the same manner of neat-fit one, Fig.13.

Fig. 16 shows an example for the effect of clearance values on the half of the contact length of 0^{o} layer. It evident that the contact length (area) decreased as the bolt-hole clearance value increased. The increase in the bolt-hole clearance from 0 to 300 µm reduces the contact area by 17.8% and accordingly, the contact pressure increased by 26.6 % as shown in Fig. 16. The increase of the contact pressure and the reduction of the contact area with increasing the bolt-hole clearance are the main reasons for increasing of hole deformation and decreasing the joint stiffness as shown in Fig. 14. Accordingly, the 4% HDS, first peak bearing strength, the measured ultimate strength and the predicted ultimate strength were decreased respectively by 20.9%, 34.0%, 14.2% and 8.8%.

Calculating the contact area and pressure on each layer was used to predict the in-situ failure mode of $[0/90]_{2S}$ GFRE bolted joint. Fig. 17 shows an example of the predicted failure mode of bolted joint with neat-fit (zero) clearance. The shear-out failure mode appears at layers with 0°orientation due to matrix failure with a tendency to net tension appears at layers of 90° orientation angle due to fiber and matrix failures. The bearing appears in both 0° and 90° layers due to matrix cracking, delamination, 0°-fiber splaying and fracture of 90°-fiber layers.

CONCLUSION

In this study, the effect of bolt-hole clearance on the performance of bolted joints in $[0/90]_{2S}$ GFRE composite was investigated experimentally and numerically. A progressive damage model was developed using the Hashin failure criteria and a property degradation rules. From this study, the following conclusion can be drawn:

- A unidirectional (UD) as well as $[0/90]_{2S}$ cross-ply GFRE composite laminates were manufactured locally using hand lay-up technique. A series of ASTM tests (tensile, compressive and shear) were conducted on a unidirectional laminates to find the lamina properties, which were used as input to a 3D developed progressive damage numerical model. The visual examination of the fractured

specimens showed that the failure modes of the various experimental tests are agreed well with those presented in the ASTM standards.

- The measured mechanical properties are agreed well with the predicted values using well-known analytical models. The measured tensile, compressive and shear strength was slightly lower than that the predicted values due to cure residual stress, which is contributed by the chemical shrinkage of the curing resin and the thermal cooling contraction of the resin and fiber system. In addition, the voids contend in the composite laminate that formed during the manufacturing process can represent as stress initiator for fiber/matrix interfacial debonding as well as crack propagation and thus, reducing the laminate strength.
- The load-displacement curve of bolted joint in $[0/90]_{2S}$ GFRE specimen showed a nonlinearity within small initial displacements until the bolt achieving full intimate contact with the hole at about 0.5 kN, and then followed by a linear relationship up to 3.6 kN. Matrix damage accompanied with delamination initiation was clearly observed at load of 2.3 kN. These damage mechanisms are progressively increased up to bearing, fiber splaying and shear-out initiations accompanied with a nonlinear behavior of the load-displacement curve at 3.6 kN. Bearing failure associated with shear-out was clearly observed at the first peak load of 5.35 kN. The fracture of the bolted joint was associated with net-tension failure mode at ultimate load of about 6.6 kN.
- Increasing the bolt-hole clearance from zero to 50 µm decreases the first peak and the ultimate strengths by 15.9 % and 6.2 %, respectively. Whereas, increasing the bolt-hole clearance from zero to 300 µm decreases the first peak and the ultimate strength by 34.0 % and 14.2 %, respectively.
- The increase in the bolt-hole clearance from 0 to 300 µm reduces the contact area by 17.8% and increasing the contact pressure by 26.6 %. Accordingly, the 4% HDS, first peak bearing strength, the measured ultimate strength and the predicted ultimate strength were decreased respectively by 20.9%, 34.0%, 14.2% and 8.8%. The numerical results of the ultimate strength of the composite bolted joints with different clearances agree well with the experimental ones with a maximum deviation of 7.1 %.
- Calculating the contact area and pressure on each layer was used to predict the in-situ failure mode of $[0/90]_{2S}$ GFRE bolted joint. The shear-out failure mode appears at layers with 0°orientation due to matrix failure with a tendency to net tension appears at layers of 90° orientation angle due to fiber and matrix failures. The bearing appears in both 0° and 90° layers due to matrix cracking, delamination, 0°-fiber splaying and fracture of 90°-fiber layers.

REFERENCES

[1] Khashaba UA, Sallam HEM, Al-Shorbagy AE, Seif MA. Effect of washer size and tightening torque on the performance of bolted joints in composite structures. Compo Struct 2006; 73:310–317.

[2] Chamis, CC. Simplified Procedure for Designing Composite Bolted Joints. J Compos Mater, 1990;9: 614-626.

[3] Giannopoulos IK, Doroni-Dawes D, Kourousis KI, Yasaee M. Effects of bolt torque tightening on the strength and fatigue life of airframe FRP laminate bolted joints. Compos Part B Eng 2017;125: 19-26.

[4] Zhai Y, Li D, Li X, Wang L, Yin Y. An experimental study on the effect of bolt-hole clearance and bolt torque on single-lap, countersunk composite joints. Compos Struct 2015;127: 411–419

[5] Khashaba UA, Sebaey TA, Alnefaie KA. Failure and reliability analysis of pinned-joints composite laminates: Effects of pin-hole clearance. J Compos Mater 2013;47: 2287–2298.

[6] Maikuma H and Kubomura K. Bearing strength damage progress for PAM-based and pitch-based carbon fiber composites. J Compos Mater 1993; 27: 1739–1761.

[7] Khashaba UA, Sebaey TA, Alnefaie KA. Failure and reliability analysis of pinned-joints composite laminates: Effects of stacking sequences. Compos Part B Eng 2013;45: 1694–1703.

[8] Herrington PD and Sabbaghian M. Effect of radial clearance between bolt and washer on the bearing strength of composite bolted joints. J Compos Mater 1992; 26: 1826–1843.

[9] Kelly G, Hallström S. Bearing strength of carbon fibre/epoxy laminates: effects of bolt-hole clearance. Compos Part B Eng 2004;35:331–343

[10] Hollmann K. Failure analysis of bolted composite joints exhibiting in-plane failure modes. J Compos Mater 1996;30(3):359–83.

[11] McCarthy MA, Lawlor VP, Stanley WF, McCarthy CT. Bolt-hole clearance effects and strength criteria in single-bolt, single-lap, composite bolted joints. Compos Sci Technol 2002;62: 1415–1431.

[12] Camanho PP, Lambert M. A design methodology for mechanically fastened joints in laminated composite materials. Compos Sci Technol 2006;66(15): 3004-20.

[13] Hyer MW, Klang EC, Cooper DE. The Effects of Pin Elasticity, Clearance, and Friction on the Stresses in a Pin-Loaded Orthotropic Plate. J Compos Mater 1987;21:190-206

[14] McCarthy CT, McCarthy MA. Three-dimensional finite element analysis of single-bolt, single-lap composite bolted joints: Part II — effect of bolt-hole clearance. Compos Struct 2005; 71: 159-175.

[15] Hu XF, Haris A, Ridha M, Tan VBC, Tay TE. Progressive failure of bolted single-lap joints of woven fibre-reinforced composites. In-Press, Compos Struct 2018.

[16] Inal O, Balıkoğlu F, Atas A. Bolted joints in quasi-unidirectional glass-fibre NCF composite laminates. Compos Struct 2018;183: 536–544.

[17] Khashaba UA, Sebaey TA, Mahmoud FF, Selmy AI, Hamouda RM, Experimental and numerical analysis of pinned-joints composite laminates: Effects of stacking sequences. J Compos Mater 2013;47: 3353–3366.

[18] Khashaba UA. Notched and pin bearing strengths of GFRP composite laminates. J Compos Mater 1996;30:2042–2055.

[19] Khashaba UA. In-plane shear properties of cross-ply laminate with different off-axis angles. Compos Struct 2004; 65: 167–177.

[20] Lawlor VP, Stanley WF, McCarthy MA. Characterisation of damage development in single-shear bolted composite joints. Plast Rubber Compos 2002;31: 126–133.

[21] McCarthy MA, Lawlor VP and Stanley WF. An experimental study of bolt–hole clearance effects in single-lap, multibolt composite joints. J Compos Mater 2005; 39: 799–825.

[22] McCarthy CT, McCarthy MA. Three-dimensional finite element analysis of single-bolt, single-lap composite bolted joints: part I—model development and validation. Compos Struct 2005; 71: 140-158
[23] F.F. Mahmoud, S.S Ali-eldin, M.M. Hassan, S.A. Emam. An incremental mathematical programming model for solving multi-phase contact problems. Comput Struct 1998;68:567-581
[24] Vangrimde B, Boukhili R. Analysis of the bearing response test for polymer matrix composite laminates: bearing stiffness measurement and simulation. Compos Struct 2002; 56: 359-374.
[25] Okutan B, Karakuzu R. The strength of pinned joints in laminated composites. Compos Sci Technol 2003; 63: 893-905.
[26] Rao SS. The finite element method in engineering. Pergamon Press, UK, 2nd Edition, 1989.
[27] Staab GH. Laminar composites. Butterworth-Heinemann Publication, USA, 1999
[28] Gibson RF. Principles of composite material mechanics. McGraw-Hill Publication, 1994.
[29] Naik NK and Kumar RS. Compressive strength of unidirectional composites: evaluation and comparison of prediction models. Compos Struct 1999; 46: 299-308.
[30] Benzarti K, Cangemi L, Dal Maso F. Transverse properties of unidirectional glass/epoxy composites: influence of fiber surface treatments. Compos Part A 2001; 32: 197-206.
[31] Gonzalez C and Llorca J. Mechanical behavior of unidirectional fiber-reinforced polymers under transverse compression: Microscopic mechanisms and modeling. Compos Sci Technol 2007; 67: 2795–2806.
[32] Bhatanagar N, Ramakrishnan N, Naik NK, Komanduri R. On the Machining of Fiber Reinforced Plastic (FRP) Composite Laminates. J Mach Tools Manufact 1995; 35(5):701–16.
[33] Baba BO. Behavior of Pin-loaded Laminated Composites. Exp Mech 2006; 46: 589–600.
[34] Zhao LG, Warrior NA, Long AC. A micromechanical study of residual stress and its effect on transverse failure in polymer–matrix composites. Int J Solids Struct 2006;43: 5449–5467.

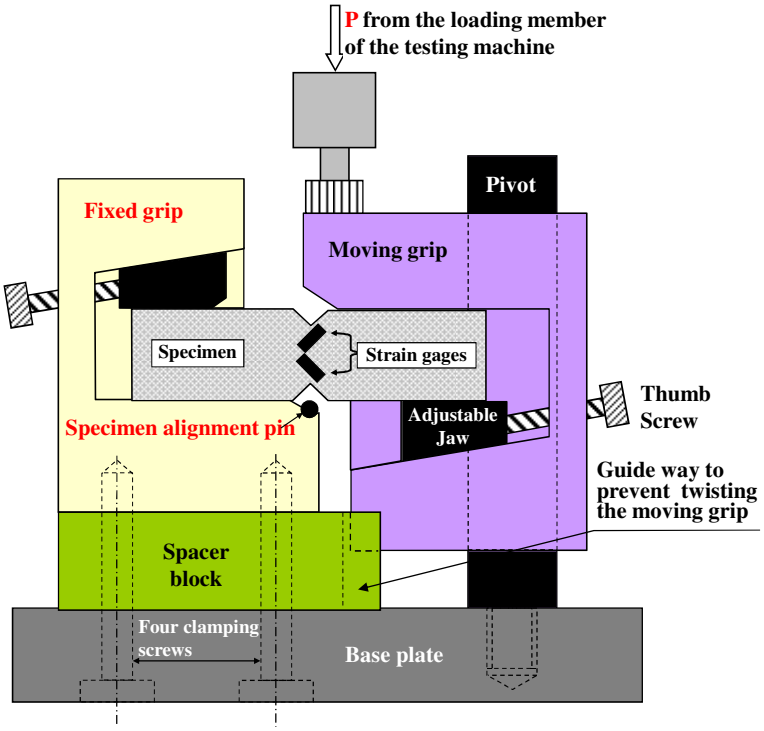

Fig. 1. Iosipescu shear tests fixture.

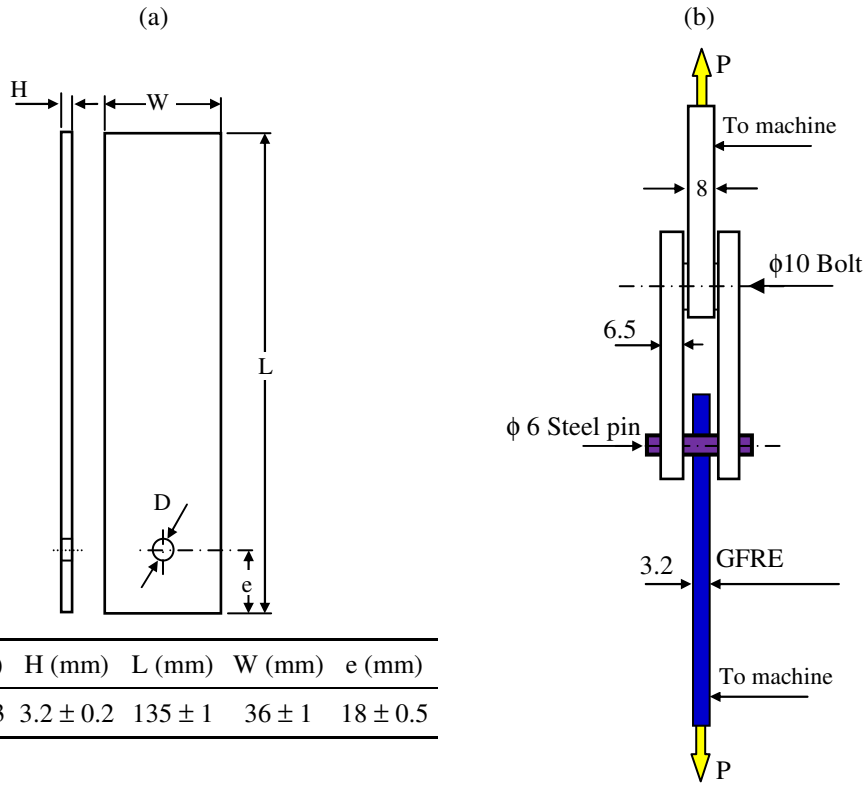

D (mm)	H (mm)	L (mm)	W (mm)	e (mm)
6 ± 0.03	3.2 ± 0.2	135 ± 1	36 ± 1	18 ± 0.5

Fig. 2. (a) Dimensions of pinned-joint specimens, and (b) Bolted joint fixture.

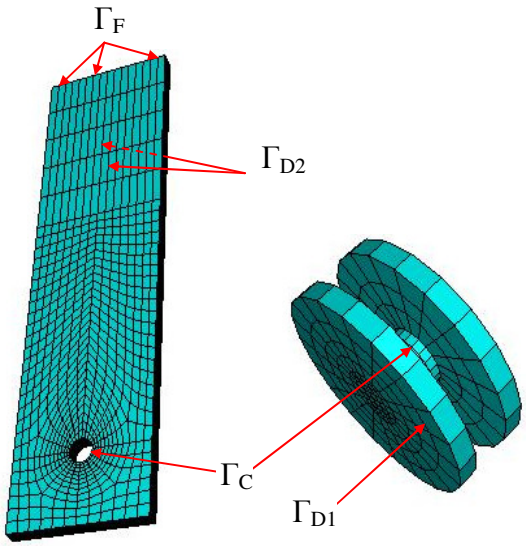

Fig. 3. Bolted joint specimen and bolt.

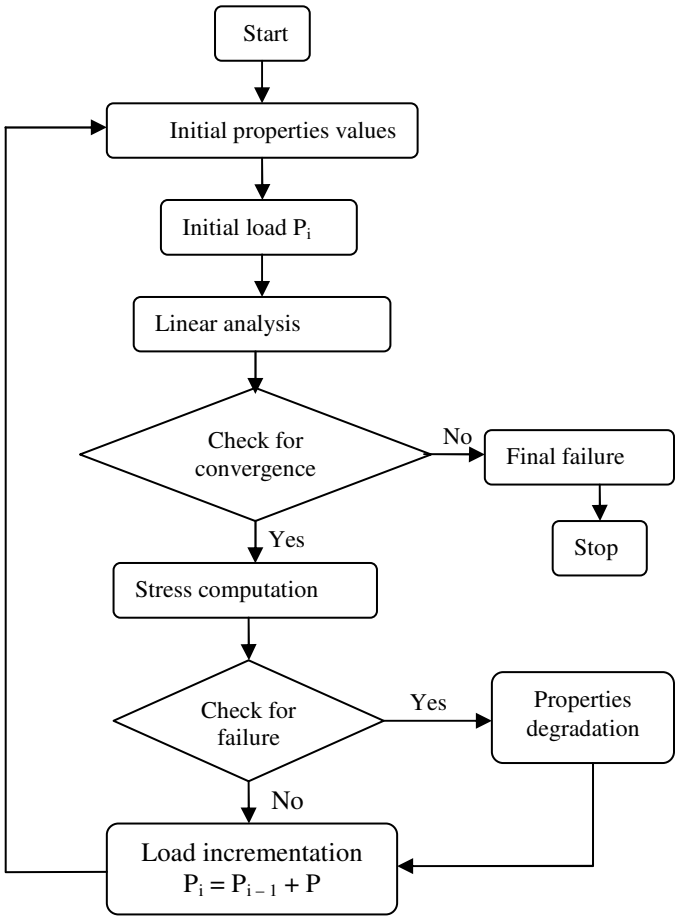

Fig. 4. Flowchart of the progressive Damage Model.

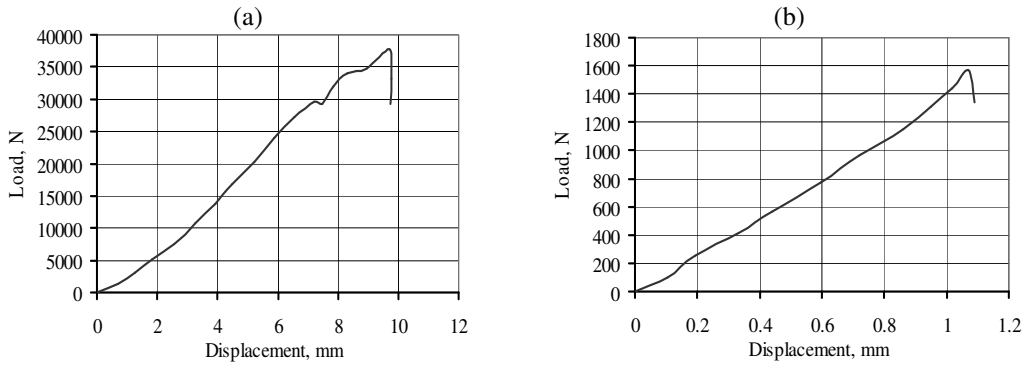

Fig. 5. Load-displacement curve of UD-GFRE tensile specimen (a) loaded in the fiber direction, (b) loaded in the transverse direction.

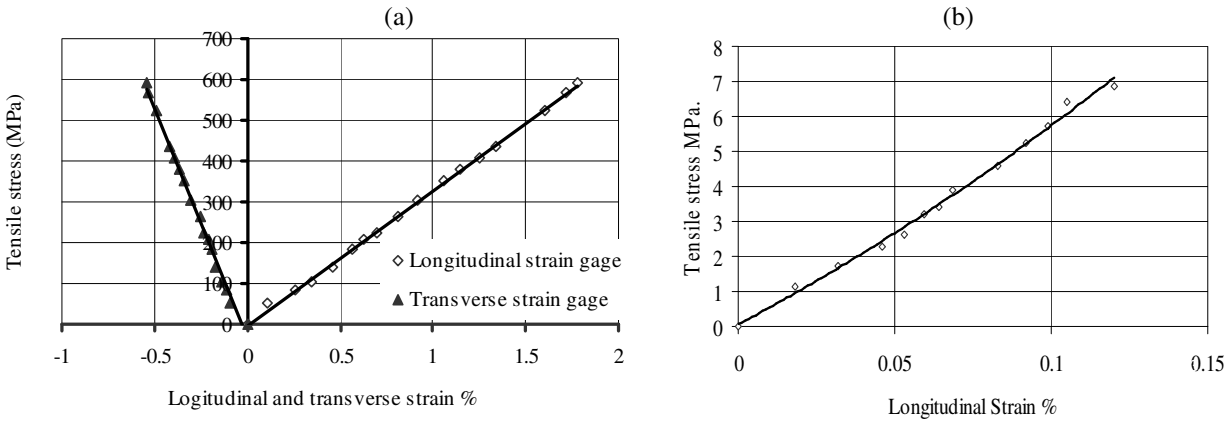

Fig. 6. Stress-strain curve of UD-GFRE tensile specimen: (a) In the fiber direction, and (b) In the transverse direction.

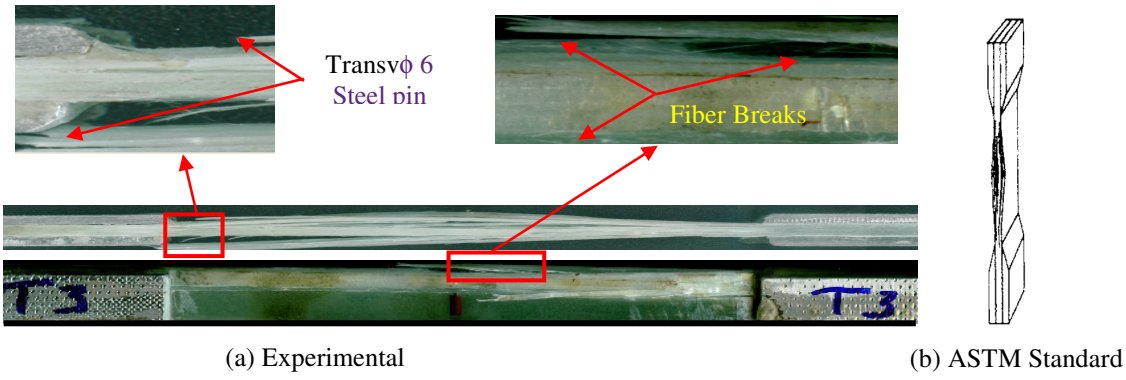

Fig. 7. (a) Image of fractured UD-GFRE specimen loaded in fiber direction, and (b) ASTM typical mode.

Fig. 8. (a) Image of fractured UD-GFRE specimen loaded in transverse direction, and (b) ASTM typical mode.

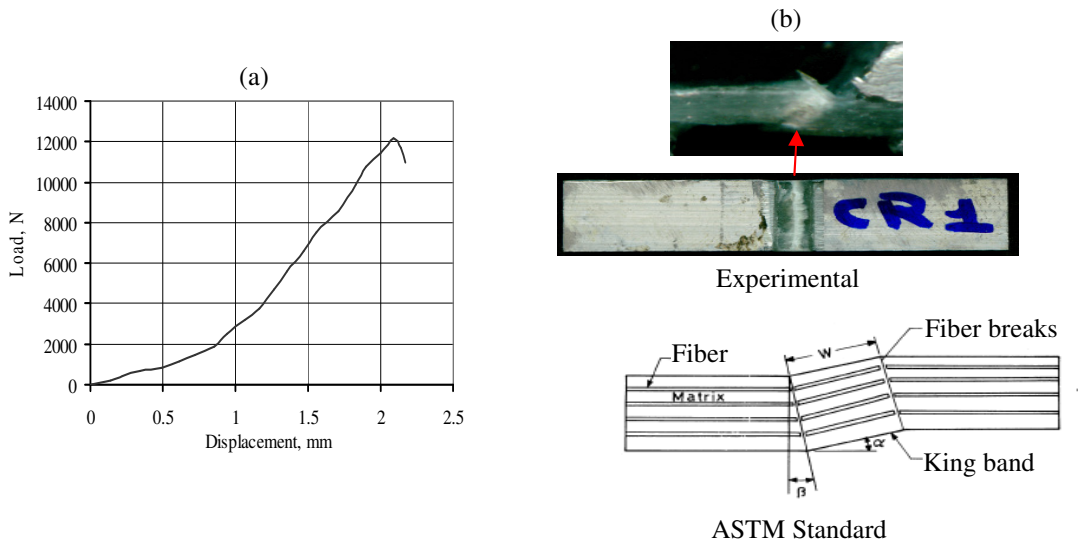

Fig. 9. (a) Load-displacement curve, and (b) failure mode of UD-GFRE compressive specimen loaded in the fiber direction and the ASTM typical failure mode.

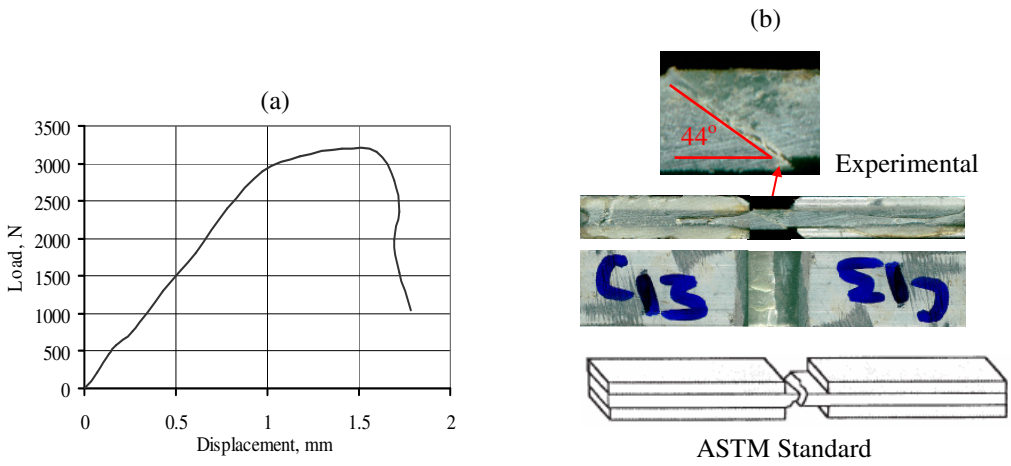

Fig. 10. (a) Load-displacement curve, and (b) failure mode of UD-GFRE specimen loaded in the transverse direction and the ASTM typical failure mode.

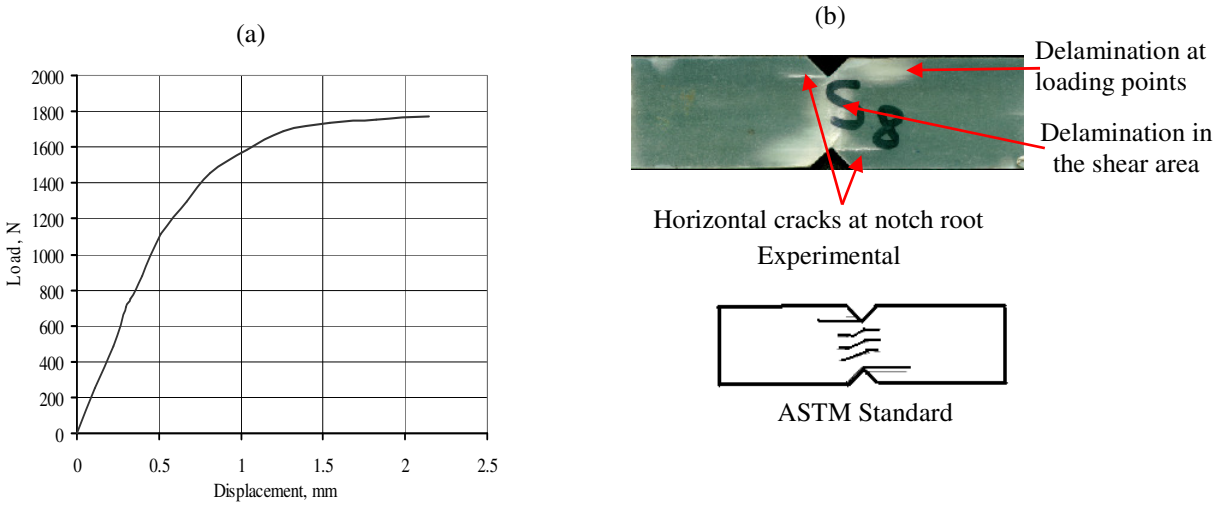

Fig. 11 (a) Load-displacement curve, and (b) failure mode of UD-GFRE shear specimen and the ASTM typical failure mode.

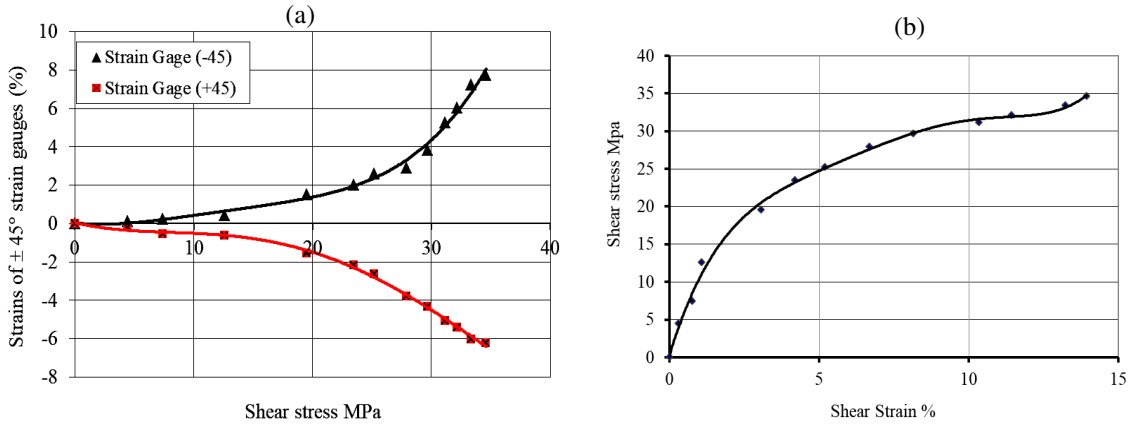

Fig. 12. (a) shear stress vs ± 45° strains, and (b) shear stress vs shear strains of UD-GFRE specimen.

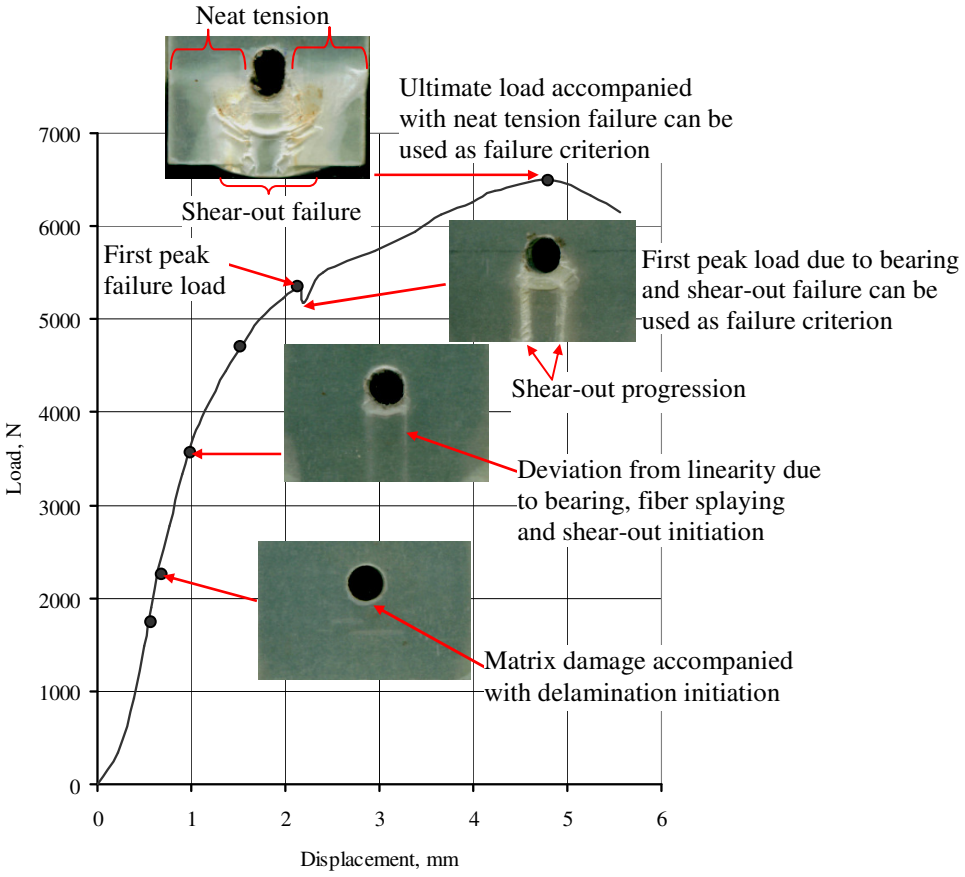

Fig. 13. Load-displacement curve of bolted joint in $[0/90]_{2S}$ GFRE composite with neat-fit clearance, C1 = 0.

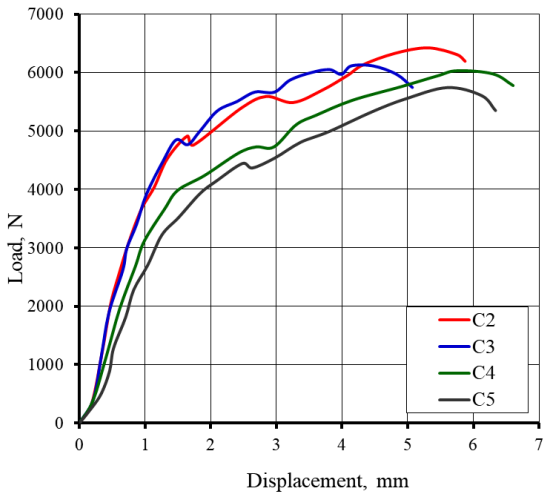

Fig. 14. Load-displacement curve of bolted joint in $[0/90]_{2S}$ GFRE composite with different clearance values.

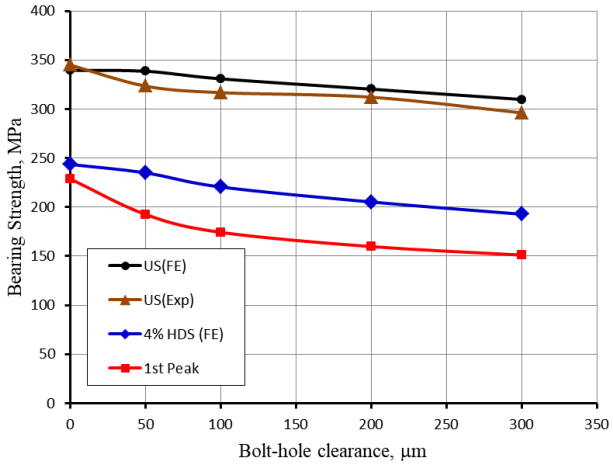

Fig. 15. Effect of bolt/hole clearance upon the bearing strength of $[0/90]_{2S}$ GFRE bolted joint specimens.

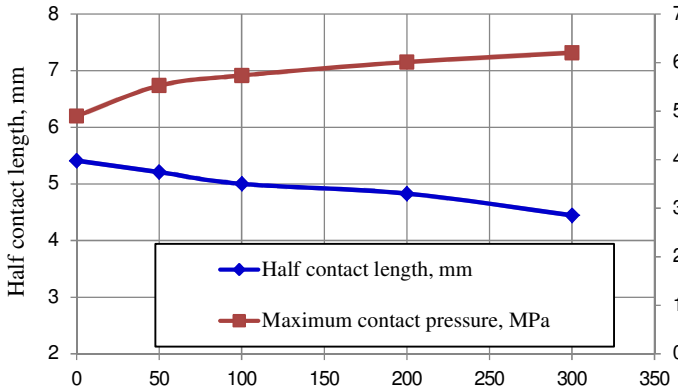

Fig. 16. Half contact length and contact pressure at failure vs clearance in 0° layer of $[0/90]_{2S}$ specimen.

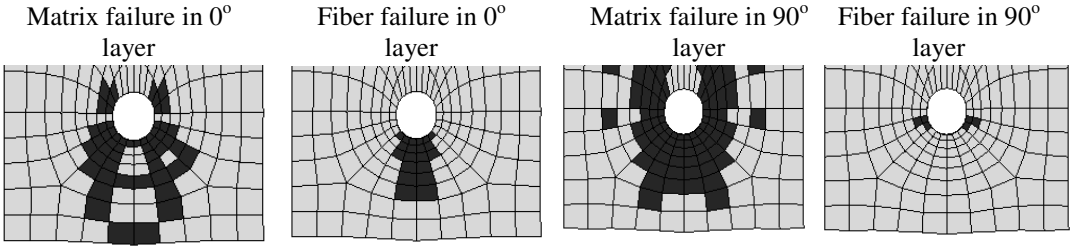

Fig. 17. Predicted failure mode of bolted joint in GFRE $[0/90]_{2S}$ laminate with neat-fit (zero clearance).